Energy evolution of channel coupling for the system ^{6}Li + ^{64}Ni at near-barrier energies

Md. Moin Shaikh[1,*] and Subinit Roy[2]
[1]*Variable Energy Cyclotron Centre, 1/AF, Bidhan Nagar, Kolkata 700064, India*
[2]*Saha Institute of Nuclear Physics, 1/AF, Bidhan Nagar, Kolkata 700064, India*

(Received 14 June 2018; published 10 August 2018)

Background: Different theoretical models have been used to understand the effects of coupling of direct reaction channels on reaction observables in recent years. However, very few attempts have been made to check the consistency of the model calculations in terms of comparing different experimental observables with the model predictions.
Purpose: In the present work, coupled channel calculations are performed with transfer and breakup coupling for collision of the weakly bound stable projectile ^{6}Li with the medium-mass target ^{64}Ni at near-barrier energies. The main goal is to find the consistency of the model calculation in simultaneous reproduction of reaction observables like the elastic angular distributions, back-angle elastic excitation function, and fusion excitation function to find the effective energy regions of dominance of these couplings.
Method: Both coupled reaction channel (CRC) and continuum discretized coupled channel (CDCC) calculations are performed using the code FRESCO. Transfer coupling is included through the CRC formalism. The CDCC scheme is used for breakup coupling and to distinguish the effect of resonant and nonresonant couplings.
Results: In the case of the CRC calculation, the full coupling including inelastic scattering, 1n stripping, and 1p stripping gives the best description of the experimental data and particularly reproduces the data in the subbarrier energy region. It is observed that the 1p-transfer channel has a larger impact on reaction observables compared to 1n transfer. On the other hand, for breakup nonresonant breakup has the dominant effect on the reaction observables, although resonant breakup has a larger cross section. The full breakup coupling reproduces the elastic scattering angular distributions and excitation function in the above-barrier region. But the scheme overpredicts these observables in the subbarrier region.
Conclusion: CRC and CDCC calculations are complementary to each other. The energy dependencies of the relevant couplings for the ^{6}Li + ^{64}Ni system around the barrier show that inelastic and transfer coupling are important at energies below the Coulomb barrier but continuum coupling is dominant in the above-barrier energy region.

DOI: 10.1103/PhysRevC.98.024610

I. INTRODUCTION

The impact of coupling to different direct reaction channels on elastic scattering and fusion reaction at near-barrier energies involving weakly bound systems is one of the prime reasons for the interest in low-energy nucleus-nucleus collisions [1–7]. The degree of influence of the couplings, however, varies with the target and the incident energy of the weakly bound projectile.

In general for weakly bound stable nuclei, like ^{6}Li with alpha separation energy $S_{\alpha} = 1.47$ MeV, the complete fusion (CF) cross section of the projectile at above-barrier energies is shown to be suppressed by a certain factor in comparison with the one-dimensional barrier penetration model (1DBPM) prediction for fusion. The magnitude of the observed suppression is higher for heavy-mass targets but it decreases with decreasing target mass or, more precisely, with decreasing charge product of the projectile and the target [8,9]. The suppression is essentially caused by breakup processes through the removal of flux from the incident channel before it reaches the effective barrier radius for fusion. A part of the lost flux can induce complete fusion by sequential capture of the two projectile fragments with the target [1]. The process cannot be distinguished experimentally [4] from the CF process where the projectile remains intact. Consequently, the total fusion (TF) cross section, defined as the sum of the cross sections of complete fusion and incomplete fusion of one of the breakup fragments of the projectile, remains more or less unaffected by the breakup process at above-barrier energies. The TF cross sections at these energies coincide with the 1DBPM predictions as well as with the coupled channel predictions for fusion cross sections.

On the other hand, at subbarrier energies, both CF and TF cross sections involving weakly bound projectiles exhibit enhancements with respect to the 1DBPM predictions. Unlike strongly bound projectiles, the enhancement of fusion cross sections of weakly bound projectiles at below-barrier energies is not very clearly understood. Whether the observed enhancement can be explained through the couplings to inelastic excitation and transfer channels or the breakup of the projectile affects the enhancement needs to be investigated. Unfortunately, no unified reaction model exists that

*md.moinshaikh1987@gmail.com

simultaneously encompasses couplings to collective excitations, transfer channels, and excitation to the continuum.

At near-barrier energies, the effect of coupling to the continuum on elastic scattering is also quite significant. Several studies have been performed spanning a wide target mass range and using weakly bound stable as well as unstable projectiles [10–23]. While Coulomb-induced coupling to the continuum dominates the elastic scattering from high-Z heavy-mass targets, the interplay of Coulomb and nuclear breakup becomes important as the target charge and mass decrease [24]. Coulomb breakup, introducing long-range absorption, affects primarily the Coulomb rainbow region of the elastic angular distribution. Nuclear breakup strongly affects the elastic phase shift and thus modifies the shape of the elastic angular distribution. In general, coupling to breakup channels introduces a repulsive real dynamic polarization potential but coupling to bound reaction channels produces an attractive real dynamic polarization potential. Effects are strong with the incident energy close to the barrier. The resultant effect on elastic scattering is of great interest.

In a recent work [25], we have investigated the effect of coupling to inelastic and one-particle transfer reaction channels on the barrier distribution from the back-angle quasielastic excitation function, a complementary measurement of the fusion excitation function for the ^{6}Li + ^{64}Ni system at near-barrier (Coulomb barrier, $V_B = 12.41$ MeV) energies. The systematic coupled reaction channel (CRC) calculation revealed that coupling to collective excitation to the first excited state of ^{64}Ni and the resonant first excited state of ^{6}Li along with coupling to one-proton and one-neutron transfer channels reproduced the quasielastic barrier distribution quite well. However, the CRC calculation could not reproduce the high-energy part of the quasielastic excitation function.

The present work attempts to identify the relative importance of bound state–to–bound state coupling and bound state–to–continuum coupling in the direct reaction products on elastic scattering and fusion observables for the ^{6}Li + ^{64}Ni system. The primary goal is to look for energy variation of the relative influence of these couplings on the reaction observables, with particular interest in describing the higher-energy behavior of the back-angle elastic excitation function. The CRC formalism has been used to investigate the effect of coupling to bound states. The continuum discretized coupled channel (CDCC) formalism has been adopted to describe the coupling between bound states and continuum states.

II. THEORETICAL FORMALISM

Both CRC and CDCC calculations for the system ^{6}Li + ^{64}Ni have been performed using the reaction code FRESCO (FRES 2.9) [26]. The code FRESCO can calculate elastic and inelastic angular distributions, reaction cross sections, and transfer (CRC)/breakup (CDCC) angular distributions along with their integrated cross section as well as fusion cross section simultaneously. The fusion cross section (σ_{fusion}) is estimated indirectly from the relation

$$\sigma_{\text{fusion}} = \sigma_{\text{reaction}} - \sigma_{\text{outgoing}}, \quad (1)$$

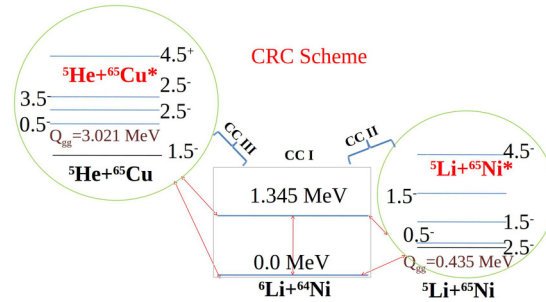

FIG. 1. Representative coupling schemes used in CRC calculation. Schemes CC I, CC II, and CC III are indicated and coupling scheme CC IV incorporates all the couplings simultaneously.

where σ_{reaction} is the total absorption cross section and σ_{outgoing} is the sum of the cross sections of individual direct reaction channels considered in the calculation.

A. CRC coupling scheme

The direct reaction channels considered in the present scheme are the inelastic excitations of the projectile ^{6}Li and the target ^{64}Ni, one-neutron stripping to the ^{5}Li + ^{65}Ni system, and one-proton stripping to the ^{5}He + ^{65}Cu system. The coupling schemes adopted in the CRC calculation are schematically shown in Fig. 1. Altogether four coupling schemes, *viz.*, CC I, CC II, CC III, and CC IV, have been used to understand the effect of coupling of direct reaction channels on different reaction observables.

Scheme CC I includes the inelastic excitations of the first excited state, 2^{+}, of the target ^{64}Ni with excitation energy 1.345 MeV and the first resonant state (3^{+}; 2.18 MeV) of the α and d cluster of the projectile ^{6}Li. Coupling scheme CC II is defined as a scheme with CC I and the one-neutron stripping channel leading to three-body final state with a Q value of 0.435 MeV. In the calculation only the ground state of the ejectile ^{5}Li and low-lying states of the residue ^{65}Ni are considered. The required spectroscopic amplitudes for the overlaps $\langle^{5}\text{Li}|^{6}\text{Li}\rangle$ and $\langle^{65}\text{Ni}|^{64}\text{Ni}\rangle$ are taken from Refs. [27,28]. To further explore the effect of one-nucleon stripping, the calculation has been performed with coupling scheme CC III. The scheme is similar to scheme CC II, with the difference that in this case the one-neutron stripping channel is replaced by a one-proton stripping channel, again leading to three-body final state, with a Q value of 3.021 MeV. The spectroscopic amplitudes associated with the $\langle^{5}\text{He}|^{6}\text{Li}\rangle$ and $\langle^{65}\text{Cu}|^{64}\text{Ni}\rangle$ overlaps are taken from Refs. [27,29].

Coupling scheme CC IV is the full channel coupling scheme, which includes the inelastic excitations of the reactants and both the one-neutron and the one-proton stripping channels.

The optical potential for the entrance channel of the ^{6}Li + ^{64}Ni system consists of a "bare" nuclear potential and the Coulomb potential with radius $R_C = 1.3 \times (A_P^{1/3} + A_T^{1/3})$ fm, where A_P and A_T are the mass numbers of the projectile and target, respectively. The real part of the bare nuclear potential is constructed by folding the density-dependent M3Y-Reid nucleon-nucleon interaction with a zero-range exchange

interaction term [30,31]. The mass densities of ^{6}Li and ^{64}Ni are taken from Refs. [30,32,33]. The imaginary component of the bare nuclear potential consists of a short-ranged volume Woods-Saxon potential that simulates the ingoing wave boundary condition [34]. The well-known Akyüz-Winther [35] potential has been used as the real potentials in the exit channels, and the same short-ranged Woods-Saxon potential with strength $W_0 = 50$ MeV, radius parameter $r_i = 1.0$ fm, and diffuseness $a_i = 0.4$ fm as the imaginary potentials. The strengths of the bound-state potentials of Woods-Saxon form, with fixed geometry parameters of radius $r_b = 1.25$ fm and diffuseness $a_b = 0.65$ fm, have been adjusted to reproduce the binding energies of the states. The transition strengths for inelastic coupling have been obtained from the deformation parameters of the projectile and target and the values of the parameters are taken from Refs. [36,37]. The details of the coupling schemes and the potential parameters can be found in Ref. [25].

B. Continuum discretized coupled channels

To observe the effect of breakup, a dominant direct reaction channel for weakly bound projectiles, CDCC calculations were performed in the measured energy range using the code FRESCO. In the calculation the projectile ^{6}Li has been taken as a two-body cluster nucleus of α and d fragments with the ground state at -1.47 MeV from the threshold. The positive energy resonant states lie in the α-d continuum. The model space has been constructed by discretizing the breakup continuum into equal energy bins in the energy space. The continuum above the $^{6}\mathrm{Li} \longrightarrow \alpha + d$ breakup threshold (1.47 MeV) is discretized into energy bins of width $\Delta E = 2$ MeV. Each bin is treated as an excited state of ^{6}Li at an excitation energy equal to the mean energy of the bin and having spin $\mathbf{J}$ and parity $(-1)^{L}$, where L is the relative orbital angular momentum between the α-particle core and the deuteron. The continuum states with $L = 0$, 1, 2, and 3 are included in the calculation. The maximum excitation energy considered for the highest incident energy is 12 MeV for all the L windows. For lower bombarding energies the upper limit of excitation is suitably modified. The widths are modified near the location of the resonant states. The resonance states considered are present at the energies 0.72, 2.84, and 4.18 MeV in the $L = 2$ continuum. The bin widths for the $L \neq 2$ continuum are kept uniform.

The cluster folding model, adopting the global α and d optical potentials with the ^{64}Ni target, has been used to generate the effective potentials in the CDCC formalism. The binding potentials between the $\alpha + d$ clusters are considered to be L dependent [38]. We have used the global α optical potentials from Refs. [39,40] in the calculation. These potentials are adjusted by renormalizing the real and imaginary strengths to match the experimental elastic scattering angular distribution data of $^{6}\mathrm{Li} + {}^{64}\mathrm{Ni}$ system at 26 MeV and the renormalization factors are $N_R = 0.70$ and $N_I = 2.50$. These renormalization factors are kept fixed for all the incident energies. The parameters for $d + {}^{64}$Ni potential are taken from Ref. [41] and are kept unmodified. In this calculation, all the reorientation couplings have been considered. Target excitation, however, is not included in the scheme. The calculations have been performed

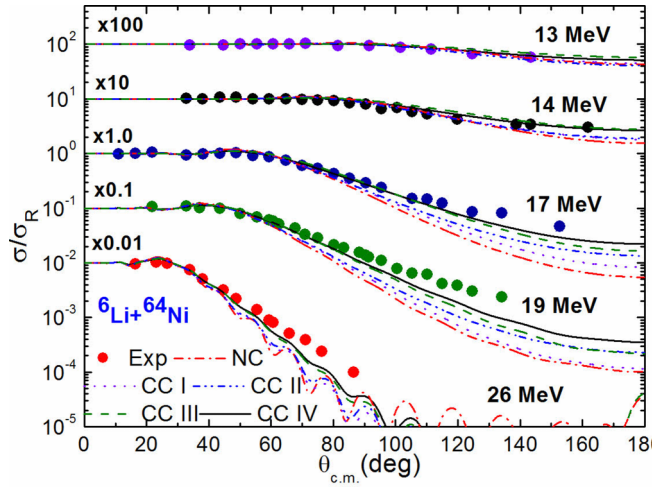

FIG. 2. Theoretical elastic scattering angular distributions obtained using different coupling schemes in CRC calculations for the system $^{6}\mathrm{Li} + {}^{64}\mathrm{Ni}$ in comparison with the experimental angular distributions taken from Ref. [33]. See text for details.

with three coupling conditions, *viz.*, first, calculation with only nonresonant continuum coupling, ignoring the presence of excited resonant states; second, calculation with coupling only to the excited resonant states; and third, calculation with the full coupling condition, which includes both resonant and nonresonant coupling terms. Calculation without any coupling has also been done for all the incident energy values.

III. RESULTS AND DISCUSSION

A. Results of CRC calculation

Measured data of the elastic angular distribution [33] at different energies, back-angle quasielastic scattering excitation function at $\theta_{\mathrm{lab}} = 150^{\circ}$ [25], and fusion excitation functions [9] are present in the literature. In the next few paragraphs, we discuss the simultaneous reproduction of the observable quantities using the CRC scheme.

Before introducing the channel coupling, a first-order distorted-wave Born approximation calculation has been performed to obtain the cross section for each channel. The corresponding output is labeled "NC." The NC cross section is used as the base for comparison of the effects of different coupling conditions on observable quantities.

To understand the reaction mechanism, the study of elastic scattering angular distributions at different energies near the barrier energy is a very useful tool. The calculated angular distributions with different coupling schemes along with the experimental data have also been plotted in Fig. 2. The benchmark angular distributions with the no-coupling condition are shown by dashed-dotted curves for all the incident energies. The angular distributions corresponding to schemes CC I, CC II, CC III, and CC IV are shown by the dotted, dashed–double-dotted, dashed, and solid curves, respectively.

It is clearly shown that the angular distributions with the no-coupling condition underpredict the experimental data at higher angles. The deviation from the measurement increases with increasing incident energy. It is also shown in Fig. 2 that

the inclusion of couplings definitely improves the reproduction of the data. A closer look at Fig. 2, however, reveals that the matching with experimental data improves significantly after the introduction of transfer coupling, and inelastic coupling alone does not have much effect on the distribution. It is also important to point out that between the transfer couplings, $1p$ stripping has a much stronger effect on the elastic scattering angular distribution compared to $1n$ transfer throughout the measured energy range. The reproduction of experimental data is best for coupling scheme CC IV, where all the above-mentioned couplings are incorporated. Scheme CC IV reproduces the experimental data at subbarrier and very close to barrier energies. But as the incident energy increases above the barrier region the calculated cross section starts to underpredict the data at higher angles. Hence, one can argue that the reproduction of elastic angular distributions from the CRC scheme is not satisfactory at higher energies, though it is quite good in the barrier and the subbarrier energy region.

As the deviation between the model predictions and the data is greater at backward angles, the effect of coupling will also be magnified at these angles. Hence, the back-angle elastic scattering excitation functions become a very useful tool to understand the effect of different couplings and the reaction mechanism. As elastic scattering and fusion are complementary to each other, coupling should affect fusion in a similar fashion. The experimental elastic scattering excitation function at back angle, $\theta_{\rm lab} = 150^\circ$ and the fusion excitation for the system ^{6}Li + ^{64}Ni have been plotted in Fig. 3 along with their theoretical counterpart.

As expected, Fig. 3(a) shows observations of the elastic scattering excitation function similar to the observations of the elastic scattering angular distribution in Fig. 2 but on a more magnified scale. The elastic scattering excitation function with the no-coupling condition greatly underpredicts the experimental data at higher energies. The deviation from the measurement decreases with decreasing incident energy. The inclusion of different couplings improves the reproduction of the data. Among all the coupling schemes, the full coupling, i.e., CC IV scheme shows the best reproduction of experimental data, although it underpredicts the experimental data at higher energies. To compare the elastic scattering excitation function with the previous observation of quasielastic scattering excitation functions [25], both the experimental and the best-fit theoretical (CC IV) quasielastic excitation functions are plotted in Fig. 3(a). It is shown that the quasielastic cross sections are slightly higher than the elastic scattering cross sections at higher energies. As the energy decreases the quasielastic scattering cross sections merge with the elastic scattering cross sections, both experimentally and theoretically, due to the dominance of the elastic scattering cross section at lower energies.

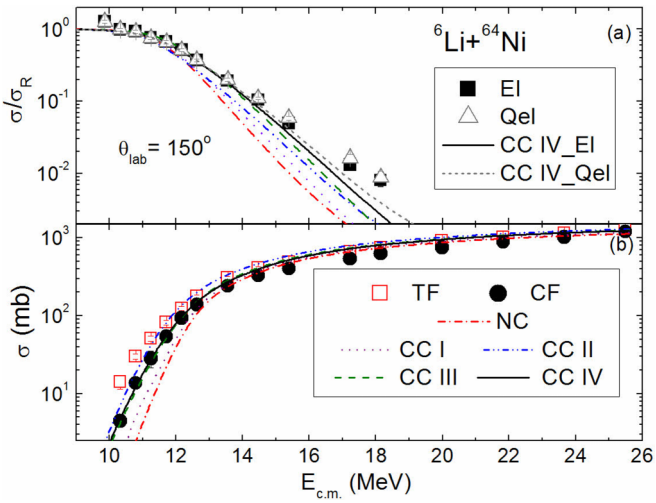

FIG. 3. Theoretical (a) back-angle elastic scattering and (b) fusion excitation functions obtained using different coupling schemes in CRC calculations for the system ^{6}Li + ^{64}Ni. Open triangles represent experimental quasielastic scattering cross sections from Ref. [25] and filled squares represent the corresponding elastic scattering cross sections. The short-dashed line is the theoretical prediction for quasielastic scattering from the CC IV coupling scheme of the CRC calculation. See text for details.

The fusion outputs of the same schemes have also been compared with the experimental fusion excitation functions, both TF and CF, in Fig. 3(b). The model fusion cross section at each energy is estimated from Eq. (1). The fusion excitation function in the no-coupling condition describes the TF data in the above-barrier region but underpredicts both CF and TF data in the below-barrier region.

With the inelastic couplings of the CC I scheme, a slight enhancement of cross sections in the subbarrier region has been observed, although no significant effect is seen in the above-barrier cross-section values.

Including the coupling of the $1n$-stripping channel along with the CC I scheme in the CC II coupling scheme produces a larger enhancement in fusion cross sections at subbarrier energies. The calculation, however, overpredicts the CF cross sections in the low-energy regime but compares well with the predictions of CC I and no-coupling conditions at above-barrier energies.

On the other hand, with the CC III coupling scheme, where the $1p$-stripping channel instead of $1n$ stripping is considered with the inelastic couplings, the model excitation function marginally underpredicts the CF data at subbarrier energies. At higher incident energies the fusion cross sections with the CC III scheme match the other model predictions indicating a reduction of the channel coupling effect.

Finally, it is observed that the CC IV coupling scheme, which includes the $1n$- and $1p$-stripping channels as well as the inelastic channels, describes CF data remarkably well at energies below the barrier. As expected it reasonably matches the cross-section values determined from other coupling schemes in the above-barrier region. All the models in this energy regime overpredict the measured CF cross sections, which are suppressed due to the effect of absorption of flux from the entrance channel by breakuplike processes.

The CRC calculations include the effects of both inelastic and transfer couplings, but not the effect of coupling to channels arising out of breakup of the projectile. In the above-barrier region, the breakup is argued to be the reason behind the suppression. The argument is corroborated by the good matching of the experimental TF excitation function with the

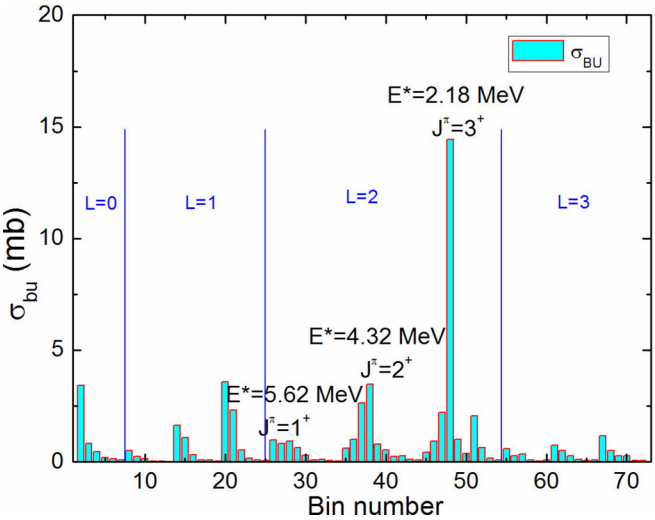

FIG. 4. Calculated breakup cross section for different excitation energies (bin) from the continuum for both resonant and nonresonant states for the system ^{6}Li + ^{64}Ni at energy 26 MeV. Bin numbers 29, 38, and 48 correspond to the resonant states 4.15, 2.88, and 0.716 MeV, respectively, in ^{6}Li, above the $\alpha + d$ threshold at 1.47 MeV with the widths 2.58, 1.85, and 0.025 MeV, respectively.

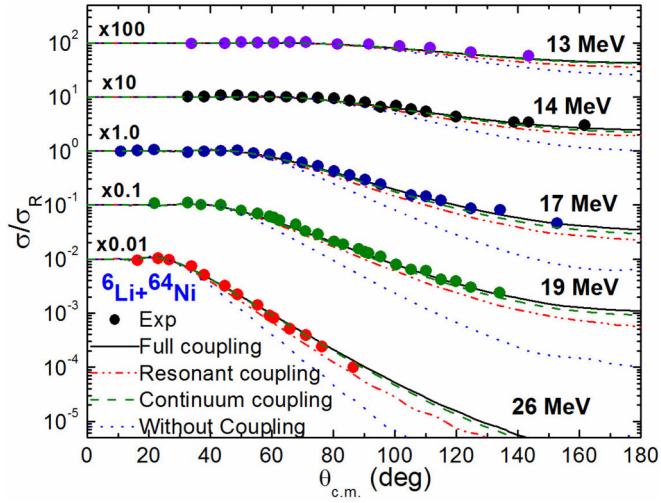

FIG. 5. Theoretical elastic scattering angular distributions calculated from CDCC calculation for the system ^{6}Li + ^{64}Ni for different coupling conditions at different energies near the barrier in comparison with the experimental angular distributions. See text for details.

1DBPM and the CRC calculations. In the below-barrier region, it has been shown in Refs. [9] and [24] that the enhancement in TF cross sections occurred because of the admixture of reactions, other than fusion. The trend observed in the CRC model description of the elastic angular distributions and excitation function as well as the fusion excitation function corroborates with the observation from the model predictions of back-angle quasielastic excitation function and the barrier distribution extracted from it as described in Ref. [25].

B. Results of the CDCC calculation

One can observe that transfer coupling is not sufficient to describe the experimental observations, especially in the higher-energy region; the effects of other dominant reaction channel breakup on different reaction observables are investigated. As already mentioned, ^{6}Li has three resonant states in the continuum. In the present case effects of nonresonant and resonant couplings are probed separately as well as simultaneously. It is reported in the literature that the major part of the breakup cross section for the projectile ^{6}Li comes from the resonant breakup of the projectile for heavy targets [10]. In Fig. 4 it is clear that this observation is also true for the projectile ^{6}Li with the medium-mass target ^{64}Ni. The breakup cross sections come mainly from the bin numbers 29, 38, and 48, which correspond to the excitation energies of 5.62, 4.32, and 2.18 MeV with resonant widths 2.58, 1.85, and 0.025 MeV, respectively. It should also be noted that bin widths are not equal for all the bins. The bin width of the continuum away from the resonance states is taken to be 2 MeV. As an example cross sections coming from bin numbers 1, 2, 3, etc., in Fig. 4 are cross sections for the 2-MeV bin width. On the other hand, the cross section in bin number 48 is only for the energy window of 25 keV. The calculated resonance energies and widths of the resonance states, above the threshold of 1.47 MeV, are quite close to their experimental values of 4.18, 2.84, and 0.716 MeV with the widths 1.5, 1.7, and 0.024 MeV, respectively.

To identify the effect of each coupling a base calculation has been performed without introducing any coupling. The curves calculated using this configuration are termed *without coupling* in different figures related to the CDCC calculation.

In Fig. 5, the calculated elastic angular distributions from CDCC calculations (i) without coupling (dotted line), (ii) with only resonant coupling (dashed–double-dotted line), (iii) with only nonresonant coupling (dashed line), and (iv) with the full coupling including both resonant and nonresonant terms (solid line) are compared with the experimental angular distributions at different incident energies. It is clearly shown in Fig. 5 that the calculated angular distributions from the no-coupling configuration underpredict the experimental data by a large amount. The description of the data improves with the inclusion of couplings but coupling only to the resonant or to the nonresonant states is not enough to describe the experimental data. Though resonant breakup is the major contributor to the total breakup cross section, its effect in terms of coupling to the entrance channel is relatively less compared to that of direct breakup to the continuum. The full coupling improves the description of the data further and the reproduction of the experimental angular distributions is quite reasonable in the measured energy range. Figure 5 clearly shows that the effect of breakup is dominant at higher incident energies as the deviation of calculated angular distributions under the no-coupling condition from the experimental data is larger in the higher-angle region at these energies.

As already mentioned, the effect of coupling is better manifested at higher angles of elastic scattering angular distributions. Following the same scheme, the back-angle excitation function has also been generated. The measured back-angle elastic scattering excitation function is compared with the

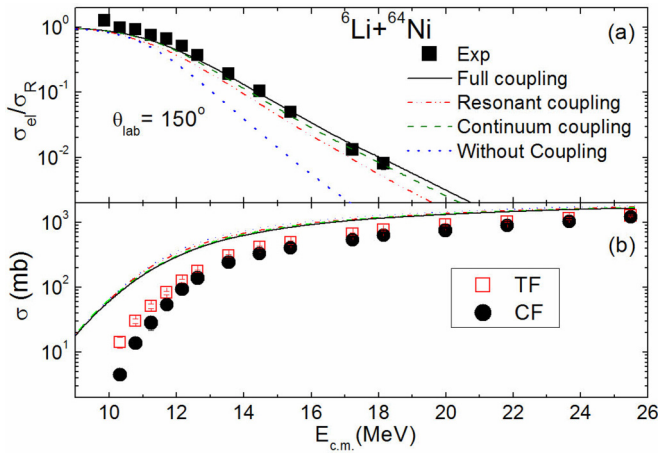

FIG. 6. Theoretical (a) back-angle elastic scattering and (b) fusion excitation functions obtained using different coupling schemes of CDCC calculations for the system ^{6}Li + ^{64}Ni in comparison with the corresponding experimental data.

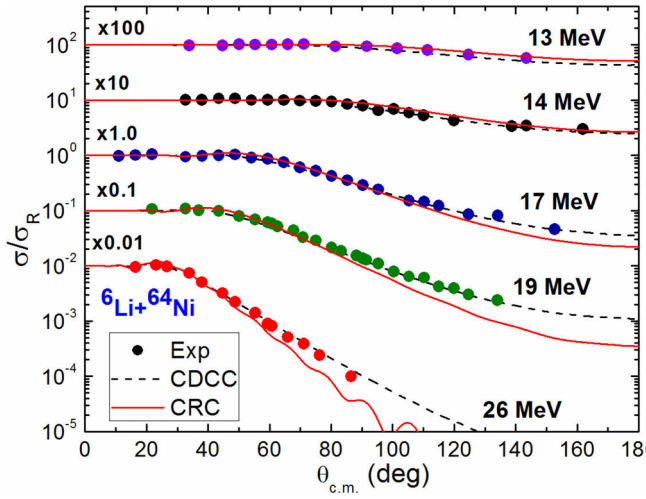

FIG. 7. Comparative elastic scattering angular distributions calculated from CRC coupling scheme CC IV and the full CDCC coupling scheme for the system ^{6}Li + ^{64}Ni.

CDCC model prediction in Fig. 6(a). The observed trend in the description of the excitation function also corroborates with the observation from the description of elastic angular distributions. The excitation function with full coupling is found to be closest to the experimental data. It is also observed that the reproduction is good at the highest energy points, and as the energy decreases the full coupling excitation function starts to underpredict the experimental values. The breakup coupling appears to be dominant at relatively higher energies and one may argue that the effects of breakup and transfer couplings on elastic scattering are complementary to each other.

The fusion excitation functions obtained from the same CDCC coupling conditions along with the experimental excitation function [9] are plotted in Fig. 6(b). The theoretical excitation functions for all conditions overestimate the measured excitation function throughout the measured energy range by a significant amount. The effect of coupling is not as striking as observed for elastic scattering. The reason behind this overestimation is embedded in the method of obtaining the fusion cross section [Eq. (1)]. The transfer channels have significant cross sections in the measured energy range. Within the CDCC formalism adopted in the present model calculation, the transfer component could not be delineated from the fusion cross section, and hence, the large enhancement. If the continuum associated with the ^{6}Li projectile can be described as a three-body $\alpha + p + n$ continuum instead of only a two-body $\alpha + d$ continuum, simultaneous estimation of the breakup and dominant one-nucleon transfer cross sections within the CDCC framework seems to be possible.

C. Comparisons

Different experimental observables, *viz.*, elastic scattering angular distribution, back angle elastic scattering, and fusion excitation function, for the system ^{6}Li + ^{64}Ni have been discussed in the light of transfer coupling (CRC) and breakup coupling (CDCC) schemes. It is observed that the introduction of couplings significantly improves the simultaneous reproduction of data compared to the respective no-coupling configurations for both schemes. But none of the schemes reproduce the experimental data over the whole energy range measured. Figures 7 and 8 reveal the relative importance and dominance of the CRC calculation with the full coupling condition in comparison with the full CDCC calculation on the observable quantities.

In Fig. 7, the angular distributions from the full CRC calculation are represented by solid lines, and those from the CDCC calculation by dashed lines. It is shown in Fig. 7 that both CRC and CDCC calculations reproduce the elastic angular distributions at Coulomb-dominated forward angles, where the effect of couplings is expected to be negligible. As we focus on the higher-angle side of angular distributions, the region dominated by the nuclear potential, we find that

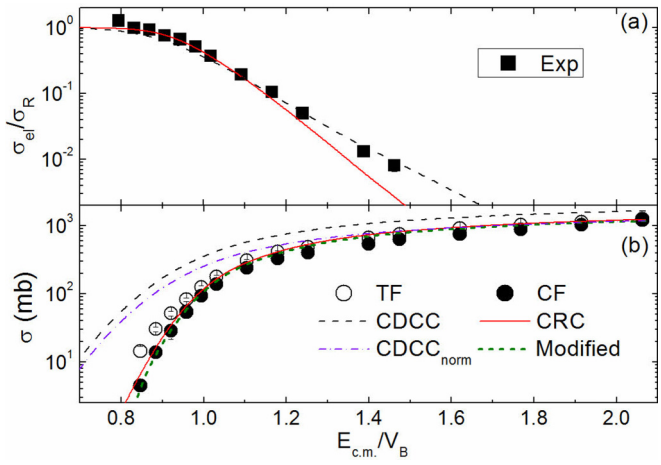

FIG. 8. Comparative (a) back-angle elastic scattering and (b) fusion excitation functions calculated for the system ^{6}Li + ^{64}Ni. The dashed-dotted curve represents the normalized CDCC excitation function and the short-dashed curve represents the realistic fusion excitation function from the code FRESCO.

the calculated angular distributions from the CRC start to deviate from experimental data with increasing angle values, especially at higher energies. The deviation diminishes with a decrease in incident energy, and below the barrier the calculation reproduces the elastic angular distributions quite nicely. On the contrary, the angular distributions predicted by the CDCC model reproduce the experimental data at higher angles and higher energies quite nicely. The calculation somehow deviates from the experimental data below the barrier energy.

The effect of coupling on elastic scattering is more clearly visualized by the back-angle elastic scattering excitation function, which is shown in Fig. 8(a). The figure clearly shows that the reproduction with the CRC model is good on the lower-energy side and it gradually underpredicts the experimental data at higher energies. The result with the CDCC calculation is just the reverse of the CRC model prediction. The CDCC reproduces the data nicely on the higher-energy side and deviates from the experimental data at lower energies. Figure 8(a) clearly indicates that the higher-energy region is dominated by breakup coupling and the influence of transfer coupling is important at lower energies. The two couplings complement each other quite nicely over the measured energy range.

If we extend our modeling to describe the fusion excitation function using both coupling schemes. It is shown in Fig. 8(b) that the excitation function from the CDCC overestimates the fusion cross sections throughout the measured energy range, whereas the cross sections from the CRC calculation overpredicts the CF cross sections at higher energies but reproduces the data nicely in the low-energy region. From the description of elastic scattering one would naively expect better reproduction of the fusion excitation function at higher energies from the CDCC calculation compared to the CRC prediction. This is not the case, primarily for two reasons: (a) unlike with elastic scattering, none of the couplings has any significant effect on fusion, particularly at high energies; and (b) the dominant transfer and target excitation cross sections in this energy region are not explicitly taken care of in the CDCC model. The second argument is even more prominent at subbarrier energies because in this energy region transfer has a greater cross section than complete fusion. To put both calculations on the same footing the fusion cross section from the CDCC is normalized to that from the CRC at higher energies. The normalized excitation function is plotted by the dashed-dotted curve in Fig. 8(b). It is shown that even the normalized excitation function is unable to reproduce the data at lower energies, indicating that breakup coupling has no significant effect at lower energies. As it was observed that breakup coupling does not have a significant effect on fusion in the measured energy range, to gain further insight we modified the fusion cross section obtained from the CRC calculation, which does not include the effect of breakup. The modified fusion cross section is generated by subtracting the breakup cross section (cross sections estimated from the CDCC) from the fusion cross section from the CRC. The modified fusion cross section is also plotted in Fig. 8(b). It is shown that the reproduction is exceptionally good throughout the measured energy regime except for a small region where both of the couplings are important.

IV. SUMMARY AND CONCLUSION

In summary, a comparative study of CRC and CDCC calculations has been performed using the computational code FRESCO to understand the effect of direct reaction channels, *viz.*, particle transfer and projectile breakup, on different observables for the system ^{6}Li + ^{64}Ni at near-barrier energies. These calculations indicate that particle transfer and breakup couplings work differently. It can easily be concluded that coupling has a positive influence when explaining the experimental observables, but neither the CRC nor the CDCC could explain all the experimental observables throughout the measured energy range. The CRC scheme reproduces the scattering data on the lower-energy side quite nicely, whereas it fails to explain the data above the barrier. On the other hand, observations for the CDCC are complementary to the observations for the CRC scheme i.e., for scattering data at higher energies this scheme is good, but not so on the lower-energy side. In the case of the fusion excitation functions, the CDCC scheme overestimate the experimental data over the whole measured energy regime. This large mismatch can be partially attributed to the definition of fusion cross section in FRESCO and the CDCC coupling scheme, which ignores inelastic excitation and transfer channels having significant cross sections. The CRC calculated fusion excitation function is very close to the experimental excitation function.

A calculation is required which can include both transfer and breakup coupling simultaneously to get their interplay and corresponding effects on reaction observables, which is a more realistic situation.

[1] L. F. Canto, P. R. S. Gomes, R. Donangelo, and M. S. Hussein, Phys. Rep. **424**, 1 (2006).
[2] N. Keeley, R. Raabe, N. Alamanos, and J. L. Sida, Prog. Part. Nucl. Sci. **59**, 579 (2007).
[3] B. B. Back, H. Esbensen, C. L. Jiang, and K. E. Rehm, Rev. Mod. Phys. **86**, 317 (2014).
[4] L. F. Canto, P. R. S. Gomes, R. Donangelo, J. Lubian, and M. S. Hussein, Phys. Rep. **596**, 1 (2015).
[5] A. Gómez Camacho, A. Diaz-Torres, P. R. S. Gomes, and J. Lubian, Phys. Rev. C **91**, 014607 (2015).
[6] A. G. Camacho, A. Diaz-Torres, P. R. S. Gomes, and J. Lubian, Phys. Rev. C **93**, 024604 (2016).
[7] A. Gómez Camacho, B. Wang, and H. Q. Zhang, Phys. Rev. C **97**, 054610 (2018).
[8] M. Dasgupta, P. R. S. Gomes, D. J. Hinde, S. B. Moraes, R. M. Anjos, A. C. Berriman, R. D. Butt, N. Carlin, J. Lubian,

C. R. Morton, J. O. Newton, and A. Szanto de Toledo, Phys. Rev. C **70**, 024606 (2004).
[9] Md. Moin Shaikh, Subinit Roy, S. Rajbanshi, M. K. Pradhan, A. Mukherjee, P. Basu, S. Pal, V. Nanal, R. G. Pillay, and A. Shrivastava, Phys. Rev. C **90**, 024615 (2014).
[10] G. R. Kelly, N. J. Davis, R. P. Ward, B. R. Fulton, G. Tungate, N. Keeley, K. Rusek, E. E. Bartosz, P. D. Cathers, D. D. Caussyn, T. L. Drummer, and K. W. Kemper, Phys. Rev. C **63**, 024601 (2000).
[11] K. Rusek, N. Alamanos, N. Keeley, V. Lapoux, and A. Pakou, Phys. Rev. C **70**, 014603 (2004).
[12] P. R. S. Gomes, I. Padron, J. O. Fernández Niello, G. V. Martí, M. D. Rodríguez, O. A. Capurro, A. J. Pacheco, J. E. Testoni, A. Arazi, J. Lubian, R. M. Anjos, L. C. Chamon, E. Crema, and M. S. Hussein, J. Phys. G **31**, S1669 (2005).
[13] C. Beck, N. Keeley, and A. Diaz-Torres, Phys. Rev. C **75**, 054605 (2007).
[14] A. M. Moro, K. Rusek, J. M. Arias, J. Gómez-Camacho, and M. Rodríguez-Gallardo, Phys. Rev. C **75**, 064607 (2007).
[15] H. Kumawat, V. Jha, B. J. Roy, V. V. Parkar, S. Santra, V. Kumar, D. Dutta, P. Shukla, L. M. Pant, A. K. Mohanty, R. K. Choudhury, and S. Kailas, Phys. Rev. C **78**, 044617 (2008).
[16] Y. Kucuk, I. Boztosun, and N. Keeley, Phys. Rev. C **79**, 067601 (2009).
[17] S. K. Pandit, V. Jha, K. Mahata, S. Santra, C. S. Palshetkar, K. Ramachandran, V. V. Parkar, A. Shrivastava, H. Kumawat, B. J. Roy, A. Chatterjee, and S. Kailas, Phys. Rev. C **84**, 031601(R) (2011).
[18] N. N. Deshmukh, S. Mukherjee, D. Patel, N. L. Singh, P. K. Rath, B. K. Nayak, D. C. Biswas, S. Santra, E. T. Mirgule, L. S. Danu, Y. K. Gupta, A. Saxena, R. K. Choudhury, R. Kumar, J. Lubian, C. C. Lopes, E. N. Cardozo, and P. R. S. Gomes, Phys. Rev. C **83**, 024607 (2011).
[19] A. Di Pietro, V. Scuderi, A. M. Moro, L. Acosta, F. Amorini, M. J. G. Borge, P. Figuera, M. Fisichella, L. M. Fraile, J. Gomez-Camacho, H. Jeppesen, M. Lattuada, I. Martel, M. Milin, A. Musumarra, M. Papa, M. G. Pellegriti, F. Perez-Bernal, R. Raabe, G. Randisi, F. Rizzo, G. Scalia, O. Tengblad, D. Torresi, A. Maira Vidal, D. Voulot, F. Wenander, and M. Zadro, Phys. Rev. C **85**, 054607 (2012).
[20] V. V. Parkar, V. Jha, S. K. Pandit, S. Santra, and S. Kailas, Phys. Rev. C **87**, 034602 (2013).
[21] D. R. Otomar, P. R. S. Gomes, J. Lubian, L. F. Canto, and M. S. Hussein, Phys. Rev. C **87**, 014615 (2013).
[22] C. S. Palshetkar *et al.*, Phys. Rev. C **89**, 064610 (2014).
[23] J. P. Fernandez-Garcia *et al.*, Phys. Rev. C **92**, 054602 (2015).
[24] A. Di Pietro *et al.*, J. Phys.: Conf. Ser. **492**, 012001 (2014).
[25] Md. Moin Shaikh, Subinit Roy, S. Rajbanshi, M. K. Pradhan, A. Mukherjee, P. Basu, S. Pal, V. Nanal, R. G. Pillay, and A. Shrivastava, Phys. Rev. C **91**, 034615 (2015).
[26] I. J. Thompson, Comp. Phys. Rep. **7**, 167 (1988).
[27] S. Cohen and D. Kurath, Nucl. Phys. A **101**, 1 (1967).
[28] J. Lee, M. B. Tsang, W. G. Lynch, M. Horoi, and S. C. Su, Phys. Rev. C **79**, 054611 (2009).
[29] D. D. Armstrong, A. G. Blair, and H. C. Thomas, Phys. Rev. **155**, 1254 (1967).
[30] G. R. Satchler and W. G. Love, Phys. Rep. **55**, 183 (1979).
[31] D. T. Khoa and W. von Oertzen, Phys. Lett. B **304**, 8 (1993); D. T. Khoa, W. von Oertzen, and H. G. Bohlen, Phys. Rev. C **49**, 1652 (1994).
[32] http://www-nds.iaea.org/RIPL-2
[33] M. Biswas, Subinit Roy, M. Sinha, M. K. Pradhan, A. Mukherjee, P. Basu, H. Majumdar, K. Ramachandran, and A. Shrivastava, Nucl. Phys. A **802**, 67 (2008).
[34] M. J. Rhoades-Brown and P. Braun-Munzinger, Phys. Lett. B **136**, 19 (1984).
[35] O. Akyüz and A. Winther, *Proceedings, International School of Physics Enrico Fermi, Course LXXVII*, edited by R. A. Broglia, R. A. Ricci, and C. H. Dasso (North-Holland, Amsterdam, 1981), p. 492.
[36] M. Zadro, P. Figuera, A. Di Pietro, M. Fisichella, M. Lattuada, T. Lönnroth, M. Milin, V. Ostashko, M. G. Pellegriti, V. Scuderi, D. Stanko, E. Strano, and D. Torresi, Phys. Rev. C **87**, 054606 (2013).
[37] B. Pritychenko, J. Choquette, M. Horoi, B. Karamy, and B. Singh, At. Data Nucl. Data Tables **98**, 798 (2012).
[38] J. A. Tostevin, F. M. Nunes, and I. J. Thompson, Phys. Rev. C **63**, 024617 (2001).
[39] V. Avrigeanu, P. E. Hodgson, and M. Avrigeanu, Phys. Rev. C **49**, 2136 (1994).
[40] Ashok Kumar, S. Kailas, Sarla Rathi, and K. Mahata, Nucl. Phys. A **776**, 105 (2006).
[41] D. Y. Pang, P. Roussel-Chomaz, H. Savajols, R. L. Varner, and R. Wolski, Phys. Rev. C **79**, 024615 (2009).